Geometric manipulation of a decoherence-free subspace in atomic ensembles

Dongni Chen,[1,2] Si Luo,[3] Ying-Dan Wang,[1,2] Stefano Chesi,[3,4,*] and Mahn-Soo Choi[5,†]

[1]*Institute of Theoretical Physics, Chinese Academy of Sciences, Beijing 100190, People's Republic of China*
[2]*School of Physical Sciences, University of Chinese Academy of Sciences, Beijing 100049, People's Republic of China*
[3]*Beijing Computational Science Research Center, Beijing 100193, People's Republic of China*
[4]*Department of Physics, Beijing Normal University, Beijing 100875, People's Republic of China*
[5]*Department of Physics, Korea University, Seoul 02841, South Korea*

(Received 15 March 2021; revised 10 October 2021; accepted 14 February 2022; published 28 February 2022)

We consider an ensemble of atoms with Λ-type level structure trapped in a single-mode cavity, and propose a geometric scheme of coherent manipulation of quantum states on the subspace of zero-energy states within the quantum Zeno subspace of the system. We find that the particular subspace inherits the decoherence-free nature of the quantum Zeno subspace and features a symmetry-protected degeneracy, fulfilling all the conditions for a universal scheme of arbitrary unitary operations on it.

DOI: 10.1103/PhysRevA.105.022627

I. INTRODUCTION

Coherent manipulation of quantum states is an essential part of various quantum technologies ranging from quantum-enhanced precision measurement to more ambitious goals, like quantum simulation and quantum information processing. While there remain considerable challenges to achieve reliable quantum-state engineering on large scales [1], a number of schemes to suppress and/or control decoherence and improve operational imperfections have been proposed and are currently under investigation. Notable examples include approaches based on decoherence-free subspaces [2–4], dynamical decoupling [5–7], quantum error correction [8–10], and holonomic manipulation [11–21]. In addition, topological approaches [22–24] have recently attracted remarkable interest, due to the highly appealing prospect of topologically protected operations. However, physical systems with robust and easily addressable topological entities are yet to be discovered or developed [25–29].

In this work, we combine the self-correcting features of geometric methods and the concept of decoherence-free subspaces. More specifically, we develop a holonomic manipulation scheme based on ensembles of atoms with Λ-type level structure, trapped in a single-mode cavity [30]. To implement universal holonomies, a crucial requirement is the degeneracy of the operational subspace (or, the equally demanding cyclic-evolution condition [14,21,31]). Here we identify a generally degenerate subspace, whose decoherence-free feature is inherited from the quantum Zeno subspace [32]. Similar systems have been popular for studies of dissipation-based quantum computation [3], quantum information processing [33–35], non-Adiabatic holonomic quantum computation [36], and generation of highly entangled states [37–44]. However, the degeneracy allowing for holonomic manipulation, not to speak of the combination with the decoherence-free character of the quantum Zeno subspace, has not been exploited in those works. By focusing on the simplest realization of our scheme, we prove the universality of the holonomic gates. Combining the self-correcting character of unitary operations implemented through geometric methods with the decoherence-free feature of this particular subspace might effectively provide a high level of fault tolerance, practically comparable to topological methods.

The rest of the article is organized as follows: Section II describes the model and examine the decoherence-free characteristics of the zero-energy subspace. Section III is devoted to the general scheme for holonomic manipulation within the zero-energy subspace. It provides explicit protocols for some common unitary operations and shows the universality of the holonomic scheme. Section IV provides an application of the scheme to generate a symmetric Dicke state. Finally, Sec. V concludes the article. To focus on the main scope of the work, we leave technical details in Appendices.

II. DEGENERATE DECOHERENCE-FREE SUBSPACE

We consider n identical atoms with Λ-type level structure [30] inside a single-mode cavity (see Fig. 1). The two ground states of each atom are denoted by $|0\rangle$ and $|1\rangle$, respectively, and the excited state by $|2\rangle$. The transition $|0\rangle \leftrightarrow |2\rangle$ is induced by the cavity photon while the transition $|1\rangle \leftrightarrow |2\rangle$ is driven resonantly by an external classical field. All atoms are assumed to be coupled to the cavity photon with a uniform strength g. We divide the atoms into two subensembles, A containing p atoms and B with the rest, and separately tune their characteristic Rabi transition amplitudes, Ω_a and Ω_b, respectively [41]. Note that atoms in each subensemble have a uniform Rabi transition amplitude (see Appendix C 2 for possible effects of finite inhomogeneity in parameters). In the

*stefano.chesi@csrc.ac.cn
†choims@korea.ac.kr

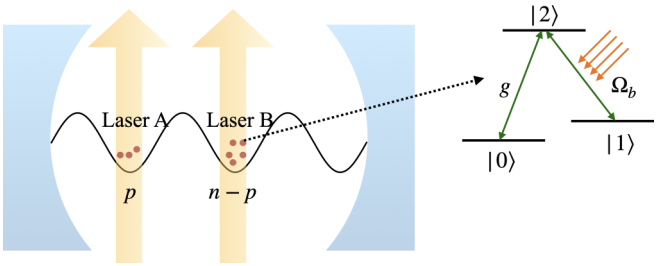

FIG. 1. Schematics of the atomic ensembles in a single-mode cavity (left), and the level structure of each atom (right).

interaction picture, the dynamics of the system is governed by the Hamiltonian $\hat{H} = \hat{H}_g + \hat{H}_\Omega$ with

$$\hat{H}_g = g\sum_{j=1}^{n} \hat{c}|2\rangle_j\langle 0| + \text{H.c.}, \tag{1a}$$

$$\hat{H}_\Omega = \Omega_a \sum_{j=1}^{p} |2\rangle_j\langle 1| + \Omega_b \sum_{j=p+1}^{n} |2\rangle_j\langle 1| + \text{H.c.}, \tag{1b}$$

where $\hat{c}$ is the annihilation operator of the cavity photon and $|s\rangle_j$ denotes the jth atom in state $|s\rangle$ ($s = 0, 1, 2$).

To identify the relevant decoherence-free subspace, we exploit the symmetries in the Hamiltonian (1): First, the total excitation number $\hat{N} = \hat{c}^\dagger\hat{c} + \sum_j(|1\rangle_j\langle 1| + |2\rangle_j\langle 2|)$ is conserved, $[\hat{N}, \hat{H}] = 0$. It allows us to focus on an invariant subspace $\mathcal{H}_N$ with a particular excitation number N. Throughout this work, the excitation number is assumed equal to the number p of atoms in subensemble A, which simplifies the initial preparation of the system. Second, the Hamiltonian is invariant under exchange of any pair of atoms within each subensemble. Among various invariant subspaces, we are mainly interested in the subspace $\mathcal{S}^A \otimes \mathcal{S}^B \subset \mathcal{H}_p$ of states which are *totally symmetric* in each subensemble. Within $\mathcal{S}_A$ or $\mathcal{S}_B$, the atoms behave like bosons. We describe the atoms in subensemble A by the bosonic operators $\hat{a}_s$ associated with the atomic levels $|s\rangle$. The atoms in B are described by similar operators $\hat{b}_s$. Expressed in terms of these bosonic operators, the Hamiltonian terms in Eq. (1) read as

$$\hat{H}_g = g(\hat{a}_2^\dagger\hat{a}_0 + \hat{b}_2^\dagger\hat{b}_0)\hat{c} + \text{H.c.} \tag{2a}$$

$$\hat{H}_\Omega = \Omega_a\hat{a}_2^\dagger\hat{a}_1 + \Omega_b\hat{b}_2^\dagger\hat{b}_1 + \text{H.c.} \tag{2b}$$

Likewise, we rewrite the conservation of the total excitation number as $\sum_{s=1}^2 \hat{a}_s^\dagger\hat{a}_s + \sum_{s=1}^2 \hat{b}_s^\dagger\hat{b}_s + \hat{c}^\dagger\hat{c} = p$, and the constraints of having a fixed number of atoms in each subensemble as $\sum_{s=0}^2 \hat{a}_s^\dagger\hat{a}_s = p$ and $\sum_{s=0}^2 \hat{b}_s^\dagger\hat{b}_s = n - p$.

Third, and most importantly, we bring into play the total occupation number in the excited level $\hat{N}_2 = \hat{a}_2^\dagger\hat{a}_2 + \hat{b}_2^\dagger\hat{b}_2$, with its associated even-odd parity operator:

$$\hat{\Pi}_2 := \exp(i\pi\hat{N}_2), \tag{3}$$

which carries an interesting "antisymmetry" [45]:

$$\{\hat{\Pi}_2, \hat{H}\} = 0. \tag{4}$$

This property follows from the fact that any atomic transition occurs through the excited level $|2\rangle$. The anti-symmetry implies that, in the parity basis, the Hamiltonian is block-off-diagonal, and leads to one of our main findings: *the zero-energy subspace of $\mathcal{S}_A \otimes \mathcal{S}_B$ is always degenerate as long as $p > 1$*. We refer to Appendix A for the details of the general proof.

Within $\mathcal{S}_A \otimes \mathcal{S}_B$, we identify a zero-energy subspace which is decoherence-free by considering the limit of quantum Zeno dynamics ($g \to \infty$). Under this condition, photon leakage out of the cavity is completely suppressed within the subspace $\mathcal{Z} \subset \mathcal{S}_A \otimes \mathcal{S}_B$ of zero-photon states, a socalled *quantum Zeno subspace* [32]. Since the coupling of atoms with the electromagnetic field is mainly to the discrete mode of the cavity, spontaneous decay from state $|2\rangle$ is also strongly suppressed [3,32,46], and $\mathcal{Z}$ can be considered as a decoherence-free subspace (see Appendix C 1 for possible effects of decoherence). Within $\mathcal{Z}$, $H_g = 0$, and the Hamiltonian $\hat{H}$ ($= \hat{H}_\Omega$) still bears the antisymmetry, Eq. (4), hence the zero-energy subspace $\mathcal{D}$ embedded in the Zeno subspace, $\mathcal{D} \subset \mathcal{Z}$, is always degenerate for $p > 1$. Besides being robust against photon decay, the states in $\mathcal{D}$ are *dynamically irresponsive* to the external driving fields, as $\hat{H}_\Omega = 0$ within $\mathcal{D}$. We call them "dark states" to distinguish them from other zero-energy states outside $\mathcal{Z}$.

In short, the subspace $\mathcal{D}$ of dark states is our desired decoherence-free subspace. Since the dark states are dynamically irresponsive, below we propose to manipulate them by geometric means, that is, using non-Abelian geometric phases (holonomies). $\mathcal{D}$ is separated by a finite energy gap ($\sim\Omega_{a/b}$) from the rest of the spectrum within $\mathcal{Z}$, hence is stable in quasiadiabatic processes.

To be specific, from now on we will focus on the case of four atoms ($n = 4$) and two excitations ($p = 2$). Then, the quantum Zeno subspace $\mathcal{Z}$ consists of the following six basis states (excluding a state which is completely decoupled from the rest):

$$\begin{aligned}
&|\zeta_1\rangle = |0020, 0\rangle, \quad |\zeta_2\rangle = |1010, 0\rangle, \quad |\zeta_3\rangle = |2000, 0\rangle,\\
&|\zeta_4\rangle = \frac{|0002, 0\rangle - |0101, 0\rangle + |0200, 0\rangle}{\sqrt{3}},\\
&|\zeta_5\rangle = \frac{|0110, 0\rangle - \sqrt{2}|0011, 0\rangle}{\sqrt{3}},\\
&|\zeta_6\rangle = \frac{|1001, 0\rangle - \sqrt{2}|1100, 0\rangle}{\sqrt{3}},
\end{aligned} \tag{5}$$

where $|n_{a_1}n_{a_2}n_{b_1}n_{b_2}, n_c\rangle$ indicate the boson numbers. Note that we have not specified the bosonic occupations of state $|0\rangle$, as they are fixed by the constraints $n_{a_0} = p - n_{a_1} - n_{a_2}$ and $n_{b_0} = n - p - n_{b_1} - n_{b_2}$. Within $\mathcal{Z}$, the matrix representation of the Hamiltonian in the specified basis is given by

$$\hat{H} \doteq \begin{pmatrix} 0 & D^\dagger \\ D & 0 \end{pmatrix} \tag{6}$$

with the off-diagonal subblock

$$D = \begin{pmatrix} -\frac{2\Omega_b}{\sqrt{3}} & \frac{\Omega_a}{\sqrt{3}} & 0 & -\Omega_b^* \\ 0 & \frac{\Omega_b}{\sqrt{3}} & -\frac{2\Omega_a}{\sqrt{3}} & -\Omega_a^* \end{pmatrix}. \tag{7}$$

It is clear that the dark-states subspace $\mathcal{D}$ is nothing but the null space of D, hence is twofold degenerate, in agreement

with our general findings. Indeed, we find the following (unnormalized) basis states spanning $\mathcal{D}$:

$$|D_1\rangle = |\zeta_1\rangle\Omega_a^2 + |\zeta_2\rangle 2\Omega_a\Omega_b + |\zeta_3\rangle\Omega_b^2 \tag{8}$$

and

$$\begin{aligned}|D_2\rangle = {} & |\zeta_1\rangle\sqrt{3}(\Omega_b^*)^2\big(3|\Omega_a|^2 + |\Omega_b|^2\big) \\ & - |\zeta_2\rangle 2\sqrt{3}\Omega_a^*\Omega_b^*\big(|\Omega_a|^2 + |\Omega_b|^2\big) \\ & + |\zeta_3\rangle\sqrt{3}(\Omega_a^*)^2\big(|\Omega_a|^2 + 3|\Omega_b|^2\big) \\ & - |\zeta_4\rangle 2\big(|\Omega_a|^4 + 4|\Omega_a\Omega_b|^2 + |\Omega_b|^4\big).\end{aligned} \tag{9}$$

III. HOLONOMIC MANIPULATIONS

With a time-dependent Hamiltonian, the quantum state acquires not only dynamical phases but also purely geometric phases, either Abelian [47] or non-Abelian [48]. Suppose that the Hamiltonian $\hat{H}(t) = \hat{H}(R_\mu(t))$ depending on slowly varying control parameters $R_\mu(t) \in \mathbb{C}$ ($\mu = 1, 2, \dots$) maintains a degenerate subspace of eigenstates $|\eta_j(R_\mu(t))\rangle$ ($j = 1, 2, \dots$) at any instant t of time. The adiabatic evolution of the states in the subspace is governed by the unitary operator (up to a global phase factor)

$$\hat{U}(t, t') = \sum_{ij} |\eta_i(R_\mu(t))\rangle U_{ij}(t, t')\langle\eta_j(R_\mu(t'))|. \tag{10}$$

The adiabatic-evolution operator $\hat{U}$ depends only on the path $\mathcal{C}$ in parameter space [48], and the corresponding unitary matrix U is given by

$$U(\mathcal{C}) = \mathcal{P}\exp\bigg(-\int_{\mathcal{C}} A^\mu dR_\mu\bigg), \tag{11}$$

where $\mathcal{P}$ denotes the path ordering and the matrix

$$A_{ij}^\mu = \langle\eta_i(R_\mu)|\frac{\partial}{\partial R_\mu}|\eta_j(R_\mu)\rangle \tag{12}$$

is the non-Abelian gauge potential describing the connection between the instantaneous bases at different points in parameter space. We will denote the non-Abelian holonomy interchangeably either by the operator $\hat{U}(\mathcal{C})$ or the matrix $U(\mathcal{C})$.

A. Amplitude and phase modulations

In our case, control parameters are the complex Rabi transition amplitudes, $\Omega_a = \Omega\sin\theta\, e^{i\phi_a}$ and $\Omega_b = \Omega\cos\theta\, e^{i\phi_b}$, and we modulate θ and ϕ_μ ($\mu = a, b$) in time. For most physical applications, $\theta = \pi/4$ ($|\Omega_a| = |\Omega_b|$) is the most interesting configuration, and many adiabatic paths either (or both) start from or end up with $\theta = \pi/4$. We find it convenient to split the path $\mathcal{C}$ into segments $\mathcal{C} = \mathcal{C}_\theta + \mathcal{C}_\phi + \mathcal{C}'_\theta + \mathcal{C}'_\phi + \cdots$. In the amplitude-modulation segments $\mathcal{C}_\theta(\theta_2, \theta_1)$, only θ is varied from θ_1 to θ_2 keeping $\phi_\mu = 0$. In the phase-modulation segments $\mathcal{C}_\phi(m_a, m_b; \theta)$, only ϕ_μ are modulated from 0 to $2\pi m_\mu$ ($m_\mu \in \mathbb{Z}$) with θ fixed.

The effects of amplitude and phase modulation are complementary: For $\mathcal{C}_\theta(\theta_1, \theta_0)$, the non-Abelian holonomy is given by (see Appendix B for technical details)

$$U(\mathcal{C}_\theta(\theta_1, \theta_0)) = \exp\{-i[c_y(\theta_1) - c_y(\theta_0)]\sigma_y\}, \tag{13}$$

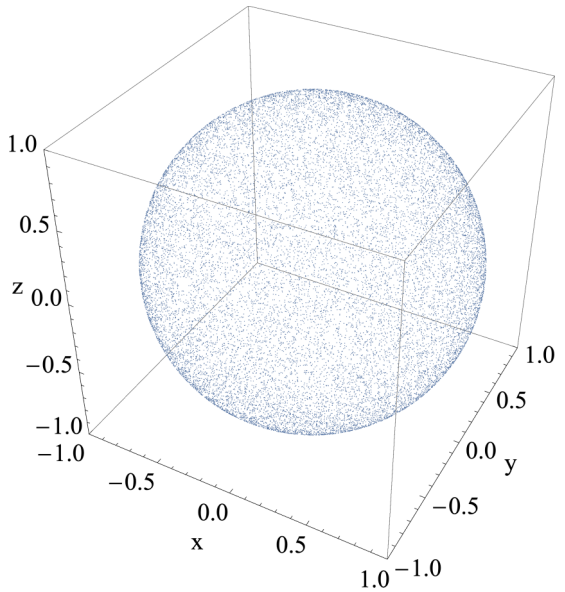

FIG. 2. Bloch sphere densely filled with states resulting from random sequences of two holonomies $\hat{U}_1$ and $\hat{U}_2$, applied to $|D_1\rangle$. We have chosen $\hat{U}_1 = \hat{U}(\mathcal{C}_\phi(1, 0; \pi/6))$ and $\hat{U}_2 = \hat{U}(\mathcal{C}_\phi(0, -1; \pi/6))$.

with $c_y(\theta) = -\arctan\sqrt{(19 - 5\cos 4\theta)/6}$, where σ^μ are the Pauli matrices in the basis of (8) and (9). $U(\mathcal{C}_\theta)$ thus describes a rotation around the fixed y axis, with only the angle depending on $\mathcal{C}_\theta$. On the other hand, $\mathcal{C}_\phi(m_a, m_b; \theta)$ gives rise to (see Appendix B)

$$U(\mathcal{C}_\phi) = \exp[ic_x\sigma_x + ic_z\sigma_z] \tag{14}$$

with the coefficients

$$\begin{aligned}c_x &= \frac{2\sqrt{6}(m_a - m_b)\pi\,\sin 2\theta\,\sin 4\theta}{(5 - \cos 4\theta)\sqrt{19 - 5\cos 4\theta)}}, \\ c_z &= \frac{(m_a + m_b)\pi(\cos 8\theta - 20\cos 4\theta + 51)}{(5 - \cos 4\theta)(5\cos 4\theta - 19)} \\ &\quad - \frac{(m_a - m_b)\pi(16\cos 6\theta - 96\cos 2\theta)}{(5 - \cos 4\theta)(5\cos 4\theta - 19)}.\end{aligned} \tag{15}$$

$U(\mathcal{C}_\phi)$ corresponds to a rotation around an axis in the xz plane with both axis and angle depending on $\mathcal{C}_\phi$.

B. Universality

Now we address the following question: Is it possible to implement an arbitrary unitary transformation by combining $\hat{U}(\mathcal{C}_\phi)$ and $\hat{U}(\mathcal{C}_\theta)$? This is a nontrivial question, as the rotation axes and angles of $\hat{U}(\mathcal{C}_\phi)$ and $\hat{U}(\mathcal{C}_\theta)$ of our concern are not continuous. However, we should recall that any two-dimensional unitary transformation can be realized to arbitrary accuracy by combining two rotations around different axes, if their angles are irrational multiples of 2π. Therefore, given a desired accuracy, we can implement any unitary transformation within $\mathcal{D}$ by combining $\hat{U}(\mathcal{C}_\phi)$ and $\hat{U}(\mathcal{C}_\theta)$. Alternatively, Fig. 2 demonstrates that two different choices of $\hat{U}(\mathcal{C}_\phi)$ are already sufficient. We have constructed random sequences of $\hat{U}_1$ and $\hat{U}_2$ of varying lengths, with $\hat{U}_1 = \hat{U}(\mathcal{C}_\phi(1, 0; \pi/6))$ and $\hat{U}_2 = \hat{U}(\mathcal{C}_\phi(0, -1; \pi/6))$, and applied them on $|D_1\rangle$. Each point in Fig. 2 represents the resulting

quantum state. As seen, the states densely fill up the Bloch sphere. The universality of holonomic manipulations within $\mathcal{D}$ of higher dimensions for more than two ensembles can be illustrated in a similar way (see Appendix B 4 and Fig. 5 in particular).

For the purpose of demonstration, we further provide explicit adiabatic paths that generate the elementary Pauli X and Z. We consider the sequence

$$\hat{W}(m_a, m_b; \theta_1) := \hat{U}(\mathcal{C}_\theta(\pi/4, \theta_1))\hat{U}(\mathcal{C}_\phi(m_a, m_b; \theta_1))\hat{U}(\mathcal{C}_\theta(\theta_1, \pi/4)). \tag{16}$$

Pauli Z is extremely simple to implement, as it is identical to $\hat{W}(1, 0; \pi/4)$.

While Pauli X cannot be implemented exactly, the following procedure enables an approximate implementation to arbitrary accuracy: First recall from Eq. (13) that $\hat{U}(\mathcal{C}_\theta(\pi/4, \theta_1)) = \hat{U}^\dagger(\mathcal{C}_\theta(\theta_1, \pi/4))$ is a rotation around the y-axis. Therefore, just like $U(\mathcal{C}_\phi)$, $\hat{W}$ is a rotation around an axis that is still in the xz plane [see Eq. (B10)]. One can numerically find a value θ_1^* such that $\hat{W}(m_a, m_b; \theta_1^*)$ is a rotation along the x axis. The rotation angle is an irrational multiple of 2π, thus $\hat{W}(m_a, m_b; \theta_1^*)$ does not yet realize the Pauli X. However, repeated applications of $\hat{W}(m_a, m_b; \theta_1^*)$ can reach any desired angle, say π, with arbitrary accuracy. This is illustrated for $m_a = 0$ and $m_b = 1$ in Fig. 4 in Appendix B 3.

IV. APPLICATION

As an example of application of our scheme, we consider the generation of symmetric Dicke states (unnormalized)

$$\left|\Phi_n^p\right\rangle = \sum_i \mathcal{P}_i |1\rangle^{\otimes p} \otimes |0\rangle^{\otimes(n-p)} \tag{17}$$

with directional "angular momentum" $(n/2 - p)$, where $\sum_i \mathcal{P}_i \cdots$ denotes the sum over distinct permutations of all n atoms. Due to their rich entanglement [49,50], Dicke states have attracted considerable interest as valuable resources, e.g., for precision measurement [51–53].

We first note that, regardless of parameters, there always exists a special dark state (unnormalized):

$$\left|E_n^p\right\rangle = (\Omega_a \hat{a}_0^\dagger - g\hat{c}\hat{a}_1^\dagger)^p (\Omega_b \hat{b}_0^\dagger - g\hat{c}\hat{b}_1^\dagger)^{n-p} (\hat{c}^\dagger)^p |\,\rangle, \tag{18}$$

where $|\,\rangle$ denotes the vacuum state (no particle at all). Interestingly, the dark state in (18) is immune to spontaneous decay from level $|2\rangle$ [54] as it does not involve the excited atomic level $|2\rangle$. A key observation is that, when $\Omega_a = \Omega_b$, $|E_n^p\rangle$ is identical to the symmetric Dicke state $|\Phi_n^p\rangle$ in the quantum Zeno limit. More specifically, considering the example of $n = 4$ and $p = 2$, $|E_n^p\rangle$ reads as (unnormalized)

$$\left|E_4^2\right\rangle = |2000, 0\rangle + 2|1010, 0\rangle + |0020, 0\rangle \tag{19}$$

in the bosonic notations or, equivalently,

$$\begin{aligned}\left|E_4^2\right\rangle = {} & |1\rangle_1|1\rangle_2|0\rangle_3|0\rangle_4 + |1\rangle_1|0\rangle_2|1\rangle_3|0\rangle_4 \\ & + |1\rangle_1|0\rangle_2|0\rangle_3|1\rangle_4 + |0\rangle_1|1\rangle_2|1\rangle_3|0\rangle_4 \\ & + |0\rangle_1|1\rangle_2|0\rangle_3|1\rangle_4 + |0\rangle_1|0\rangle_2|1\rangle_3|1\rangle_4\end{aligned} \tag{20}$$

in the traditional representation.

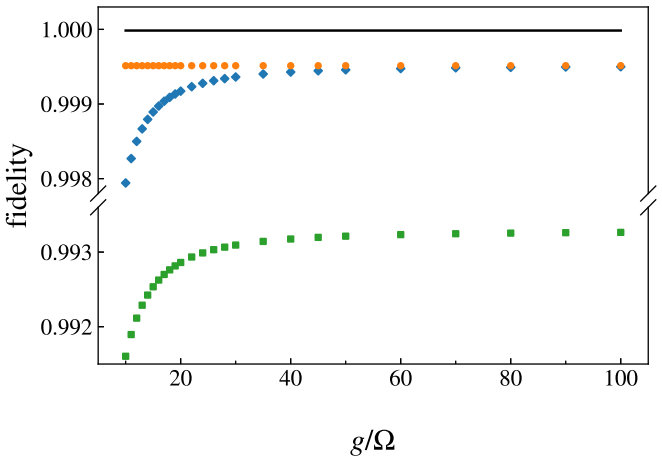

FIG. 3. Fidelity as a function of g between the desired Dicke state and the state from the adiabatic evolution $\hat{W}'(-24, 1; 0.669)$ (black solid line). We also compute the fidelity by numerically solving the Schrödinger equation along the path $\mathcal{C}_\theta(\pi/4, \theta_1) + \mathcal{C}_\phi(-24, 1; \theta_1) + \mathcal{C}_\theta(\theta_1, 0)$ within $\mathcal{Z}$ (orange filled circles) and in the whole $\mathcal{S}_A \otimes \mathcal{S}_B$ (blue filled diamonds), where $\theta_1 = 0.669$. For comparison, the fidelity of the state from the simulation along the path $\mathcal{C}_\theta(\pi/4, 0)$ is also shown with green filled squares. The discrepancy between the data sets marked with orange circles and black solid line is due to the finite simulation time, $T = 8000/\Omega$.

We want to generate the dark state in (20) [or equivalently (19)] starting from a product state $|1\rangle_1|1\rangle_2|0\rangle_3|0\rangle_4$. Note that both the initial product state and the desired dark state in (20) belong to $\mathcal{D}$, the former for $\Omega_a = 0$ and $\Omega_b = \Omega$ and the latter for $\Omega_a = \Omega_b = \Omega/\sqrt{2}$. That is, the two states are adiabatically connected and can be transformed into each other by the non-Abelian holonomy discussed above. To this end, we slightly modify the sequence in (B12) to

$$\hat{W}'(m_a, m_b; \theta_1) := \hat{U}(\mathcal{C}_\theta(\pi/4, \theta_1))\hat{U}(\mathcal{C}_\phi(m_a, m_b; \theta_1))\hat{U}(\mathcal{C}_\theta(\theta_1, 0)). \tag{21}$$

In this sequence, θ starts from 0 and moves to θ_1, then ϕ_μ make round trips from 0 to integer multiples of 2π, keeping $\theta = \theta_1$, and finally θ moves from θ_1 to $\pi/4$, where the Hamiltonian becomes symmetric between subensembles A and B. We find that the adiabatic paths specified by the parameters $\{m_a, m_b\} = \{-24, 1\}$, and $\theta_1 = 0.669$ in the sequence (21) brings the initial product state to the symmetric Dicke state in (20) with fidelity close to 1.

We also performed a time-dependent simulation with finite ramping time of the parameters, by numerically solving the Schrödinger equation in the whole space $\mathcal{S}_A \otimes \mathcal{S}_B$ (not restricted to $\mathcal{D}$ or $\mathcal{Z}$). As shown in Fig. 3, the simulation results agree very well with the holonomic treatment, as long as $g/\Omega > 10$. This implies that, protected by a finite energy gap in the spectrum, our holonomic method in the adiabatic limit can be performed at realistic speeds. The preparation time is only limited by the adiabatic condition, which is governed by the energy gap and hence by the Rabi transition amplitudes. That is, it is constant regardless of the number of atoms or ensembles.

We remark that it was previously proposed to achieve the same goal solely based on the quantum Zeno dynamics [38], which effectively corresponds to skipping the phase modulation sequence $\mathcal{C}_\phi$ in Eq. (21). This approach also assumes a finite detuning in the classical driving fields, which lifts the degeneracy in $\mathcal{D}$ and suppresses unwanted transitions to other states. In the absence of detuning, however, transitions within $\mathcal{D}$ degrade the fidelity of the final state with the desired target state. The comparison in Fig. 3 shows that the phase modulation path $\mathcal{C}_\phi$ plays a significant role to readjust the state to the desired target state.

V. CONCLUSION

In conclusion, we have considered a system of atoms with Λ-type level structure trapped in a single-mode cavity, and proposed a geometric scheme of coherent manipulation on the subspace of zero-energy states within the quantum Zeno subspace. These states inherit the decoherence-free nature of the quantum Zeno subspace and feature a symmetry-protected generic degeneracy, fulfilling all the conditions for a universal scheme of arbitrary unitary operations on it. Here we have taken a specific example with $n = 4$ and $p = 2$ for the purpose of demonstration of the main idea. However, this case can be extended in a systematic manner keeping $p = 2$ as explained in Appendix A.

ACKNOWLEDGMENTS

Y.-D.W. acknowledges support by the National Key R&D Program of China under Grant No. 2017YFA0304503, and the Peng Huanwu Theoretical Physics Renovation Center under Grant No. 12047503. S.C. acknowledges support from NSFC (Grants No. 11974040 and No. 12150610464), and NSAF (Grant No. U1930402). M.-S.C. has been supported by the National Research Function (NRF) of Korea (Grants No. 2017R1E1A1A03070681 and No. 2018R1A4A1024157) and by the Ministry of Education through the BK21 Four program.

APPENDIX A: DEGENERACY

Here we establish the generic properties of the zero-energy subspace in our system, especially the symmetry-protected degeneracy. Recall that the total number of excitations is conserved, so we focus on the subspace $\mathcal{H}_p$ with a fixed number p of excitations. There are q atoms either in state $|1\rangle$ or $|2\rangle$ and $p-q$ photons inside the cavity. This leads to the dimension of $\mathcal{H}_p$,

$$\dim \mathcal{H}_p = \sum_{q=0}^{p} 2^q \binom{n}{q}. \tag{A1}$$

We start by pointing out that there always exists a zero-energy state, regardless of the system parameters and the partition of the ensemble. The zero-energy state originates from the parity antisymmetry discussed in the main text, $\{\hat{\Pi}_2, \hat{H}\} = 0$, which implies that when we decompose $\mathcal{H}_p$ according the parity,

$$\mathcal{H}_p = \mathcal{H}_p^{\text{even}} \oplus \mathcal{H}_p^{\text{odd}}, \tag{A2}$$

the two subspaces are exclusively connected by the Hamiltonian:

$$\hat{H}\mathcal{H}_p^{\text{even}} = \mathcal{H}_p^{\text{odd}}, \quad \hat{H}\mathcal{H}_p^{\text{odd}} = \mathcal{H}_p^{\text{even}}. \tag{A3}$$

Physically, it means that whenever $\hat{H}$ induces a transition, the even-odd parity of atoms in state $|2\rangle$ will change, because any atomic transition can only occur through the excited level $|2\rangle$. Hence, the matrix representation of the Hamiltonian is block-off-diagonal in the parity basis

$$\hat{H} \doteq \begin{pmatrix} 0 & D^\dagger \\ D & 0 \end{pmatrix}. \tag{A4}$$

Now note that the dimensions of the two subspaces $\mathcal{H}_p^{\text{even/odd}}$ satisfy

$$\dim \mathcal{H}_p^{\text{even}} = 1 + \dim \mathcal{H}_p^{\text{odd}}. \tag{A5}$$

The additional 1 is attributed to the state $|p\rangle_c$, where all atoms are in the $|0\rangle$ state and the photon occupation of the cavity is p. Since the subspace of zero-energy states is nothing but the null space of subblock D, whose rank is less than $\dim \mathcal{H}_p^{\text{odd}}$, there must exit at least one zero-energy state in $\mathcal{H}_p$.

Now we turn to the partitioning of the ensemble into two subensembles A and B. In particular, we consider the subspace $(\mathcal{S}_A \otimes \mathcal{S}_B)_p \subset \mathcal{H}_p$ consisting of *totally symmetric* states under the exchange of atoms within each subensemble. As before, we decompose the subspace $(\mathcal{S}_A \otimes \mathcal{S}_B)_p$ into parity subspaces,

$$(\mathcal{S}_A \otimes \mathcal{S}_B)_p = (\mathcal{S}_A \otimes \mathcal{S}_B)^{\text{even}} + (\mathcal{S}_A \otimes \mathcal{S}_B)^{\text{odd}}. \tag{A6}$$

In the parity basis, the Hamiltonian within $(\mathcal{S}_A \otimes \mathcal{S}_B)_p$ is still block-off-diagonal as in (A4). In this case, the difference in the dimensions is bigger than 2 for $p > 1$,

$$\dim(\mathcal{S}_A \otimes \mathcal{S}_B)_p^{\text{even}} - \dim(\mathcal{S}_A \otimes \mathcal{S}_B)_p^{\text{odd}} \geqslant 2. \tag{A7}$$

It implies that the null space of the subblock D in (A4)—the subspace of zero-energy states in $(\mathcal{S}_A \otimes \mathcal{S}_B)_p$—is at least two dimensional. For example, the case with $n = 4$ and $p = 2$ has

$$\dim(\mathcal{S}_A \otimes \mathcal{S}_B)_p^{\text{even}} = 9, \quad \dim(\mathcal{S}_A \otimes \mathcal{S}_B)_p^{\text{odd}} = 6. \tag{A8}$$

For $n = 6$ and $p = 3$ case, one has

$$\dim(\mathcal{S}_A \otimes \mathcal{S}_B)_p^{\text{even}} = 19, \quad \dim(\mathcal{S}_A \otimes \mathcal{S}_B)_p^{\text{odd}} = 16. \tag{A9}$$

Therefore, in both cases, the zero-energy states are, at least, threefold degenerate.

The same principle not only applies to the quantum Zeno subspace $\mathcal{Z}$ and the zero-energy subspace $\mathcal{D}$ but is also generalized to more than two subensembles. The degeneracy-counting rule is especially simple when there are two excitations, $p = 2$. Suppose that we partition the system into M subensembles. Each subensemble contains two or more atoms; the argument below holds for an otherwise arbitrary number of atoms. By combinatorial inspection, one can show that

$$\dim \mathcal{Z}^{\text{even}} = M^2 + 1, \quad \dim \mathcal{Z}^{\text{odd}} = M(M-1), \tag{A10}$$

and

$$\dim \mathcal{Z} = \dim \mathcal{Z}^{\text{even}} + \dim \mathcal{Z}^{\text{odd}} = 2M^2 - M + 1. \tag{A11}$$

It means that the dimension of the zero-energy subspace $\mathcal{D}$ is given by

$$\dim \mathcal{D} = M + 1. \tag{A12}$$

Among the zero-energy states in $\mathcal{D}$, there is one and only one state that is "inert" in the sense that is completely decoupled from other state in the Rabi-driving Hamiltonian $\hat{H}_\Omega$. For $M = 2$ as an example, the (unnormalized) inert zero-energy state is given by

$$|0200, 0\rangle + |0101, 0\rangle 2 + |0002, 0\rangle - |0000, 2\rangle\sqrt{9/2}, \tag{A13}$$

where $|n_{a1}n_{a2}n_{b1}n_{b2}, n_c\rangle$ indicates the occupation numbers as in Eq. (5) of the main text. Excluding such an inert zero-energy state, the *effective* dimension of $\mathcal{D}$ is thus solely determined by the number of subensembles M in the system.

APPENDIX B: HOLONOMIC MANIPULATION

Here we derive explicitly the non-Abelian geometric phases within the subspace $\mathcal{D}$, starting from the case of $M = 2$ ensembles with two excitations ($p = 2$). Recall that, in our case, control parameters are the complex Rabi transition amplitudes,

$$\Omega_a = \Omega \sin\theta\, e^{i\phi_a}, \quad \Omega_b = \Omega \cos\theta\, e^{i\phi_b}, \tag{B1}$$

and we modulate θ and ϕ_μ ($\mu = a, b$) in time. As explained in the main text, we split the adiabatic path $\mathcal{C}$ into segments $\mathcal{C} = \mathcal{C}_\theta + \mathcal{C}_\phi + \mathcal{C}'_\theta + \mathcal{C}'_\phi + \cdots$. In the amplitude-modulation segments $\mathcal{C}_\theta(\theta_2, \theta_1)$, only θ is varied from θ_1 to θ_2, keeping $\phi_\mu = 0$. In the phase-modulation segments $\mathcal{C}_\phi(m_a, m_b; \theta)$, only ϕ_μ are modulated from 0 to $2\pi m_\mu$ ($m_\mu \in \mathbb{Z}$) with θ fixed. $\mathcal{C}_\phi$ is always closed, but not necessarily so is $\mathcal{C}_\theta$.

1. Amplitude modulations

We first examine the effect of an amplitude modulation along path $\mathcal{C}_\theta(\theta_1, \theta_0)$ in parameter space. The basis states in Eqs. (8) and (9) of the main text, with $\Omega_a = \Omega \sin\theta$ and $\Omega_b = \Omega\cos\theta$, directly lead to the non-Abelian gauge potential

$$A^\theta = -i\frac{2\sqrt{6}\sin 4\theta}{(5 - \cos 4\theta)\sqrt{19 - 5\cos 4\theta}}\sigma_y. \tag{B2}$$

Accordingly, the non-Abelian holonomy for $\mathcal{C}_\theta(\theta_1, \theta_0)$ is given by

$$U(\mathcal{C}_\theta(\theta_1, \theta_0)) = \exp\{-i[c_y(\theta_1) - c_y(\theta_0)]\sigma_y\} \tag{B3}$$

with

$$c_y(\theta) = -\arctan\sqrt{\frac{19 - 5\cos 4\theta}{6}}. \tag{B4}$$

2. Phase modulations

Let us now turn to the phase modulations. In this case, the non-Abelian gauge potential in Eq. (12) of the main text is not available in closed form. Then, we derive the non-Abelian geometric phase for the class of straight-line paths by means of a canonical transformation.

In the rotating frame associated with the unitary operator

$$\hat{V} := \exp[-i\phi_a(t)\hat{a}_1^\dagger\hat{a}_1 - i\phi_b(t)\hat{b}_1^\dagger\hat{b}_1], \tag{B5}$$

the Hamiltonian in Eq. (2) of the main text (recall that $\hat{H}_g = 0$ within $\mathcal{Z}$) becomes

$$\hat{H}' = \hat{H}'_\Omega - \dot{\phi}_a\hat{a}_1^\dagger\hat{a}_1 - \dot{\phi}_b\hat{b}_1^\dagger\hat{b}_1, \tag{B6}$$

where $\hat{H}'_\Omega := \hat{V}^\dagger\hat{H}_\Omega\hat{V}$ is now time-independent and reads

$$\hat{H}'_\Omega = \Omega\sin\theta\,\hat{a}_2^\dagger\hat{a}_1 + \Omega\cos\theta\,\hat{b}_2^\dagger\hat{b}_1 + \text{H.c.} \tag{B7}$$

As long as both $\phi_\mu(t)$ are linear in time, the whole Hamiltonian $\hat{H}'$ becomes time independent and can be solved exactly. Accordingly, we set

$$\phi_\mu(t) = 2\pi m_\mu t/\tau, \tag{B8}$$

where m_a and m_b are coprimes and $\tau \to \infty$ in the adiabatic limit. On this account, a phase modulation path, $\mathcal{C}_\phi(m_\mu; \theta)$, is specified by the integer parameters m_μ and the fixed amplitude θ. Note that, although in Eq. (B8) we have specified the path $\mathcal{C}_\phi(m_\mu; \theta)$ by means of an explicit parametrization, the resulting non-Abelian geometric phase holds for the given path regardless of the specific parametrization (i.e., the dependence does not need to be linear in t).

Given $\mathcal{C}_\phi(m_\mu; \theta)$, one can now solve the time-independent Hamiltonian $\hat{H}'$ in Eq. (B6), to obtain the non-Abelian geometric phase in a closed form,

$$U(\mathcal{C}_\phi) = \exp[2\pi i\langle D'_i|(m_a\hat{a}_1^\dagger\hat{a}_1 + m_b\hat{b}_1^\dagger\hat{b}_1)|D'_j\rangle], \tag{B9}$$

where $|D'_j(t)\rangle := \hat{V}^\dagger(t)|D_j(t)\rangle$ are the basis states in the rotating frame. Combining the expressions of the basis states in Eqs. (8) and (9) of the main text with Eq. (B9), one gets the following non-Abelian geometric phase along the path $\mathcal{C}_\phi(m_a, m_b; \theta)$:

$$U(\mathcal{C}_\phi) = \exp[ic_x\sigma_x + ic_z\sigma_z] \tag{B10}$$

with the coefficients

$$\begin{aligned} c_x &= \frac{2\sqrt{6}(m_a - m_b)\pi\sin 2\theta\sin 4\theta}{(5 - \cos 4\theta)\sqrt{19 - 5\cos 4\theta)}}, \\ c_z &= \frac{(m_a + m_b)\pi(\cos 8\theta - 20\cos 4\theta + 51)}{(5 - \cos 4\theta)(5\cos 4\theta - 19)} \\ &\quad - \frac{(m_a - m_b)\pi(16\cos 6\theta - 96\cos 2\theta)}{(5 - \cos 4\theta)(5\cos 4\theta - 19)}. \end{aligned} \tag{B11}$$

3. Pauli X operation

Here we demonstrate that the Pauli X operation can be implemented to an arbitrary accuracy using the sequence [Eq. (16) in the main text]

$$\begin{aligned} W(m_a, m_b; \theta_1) &:= U(\mathcal{C}_\theta(\pi/4, \theta_1)) \\ &\quad \times U(\mathcal{C}_\phi(m_a, m_b; \theta_1))U(\mathcal{C}_\theta(\theta_1, \pi/4)). \end{aligned} \tag{B12}$$

As explained in the main text, $W(m_a, m_b; \theta_1)$ is a rotation around an axis in the xz plane. By adjusting θ_1, one can make the rotation axis be aligned with the x axis. We find that, in general, the proper value θ_1^* is an irrational number ($\theta_1^* \approx 0.17$ for the simple choice $m_a = 0$, $m_b = 1$). Since Pauli X corresponds to a rotation around the x axis by an angle π, we need to adjust the other parameters to get the proper rotation angle. Unfortunately, a single application of the sequence $W(m_a, m_b; \theta_1^*)$ does not provide the

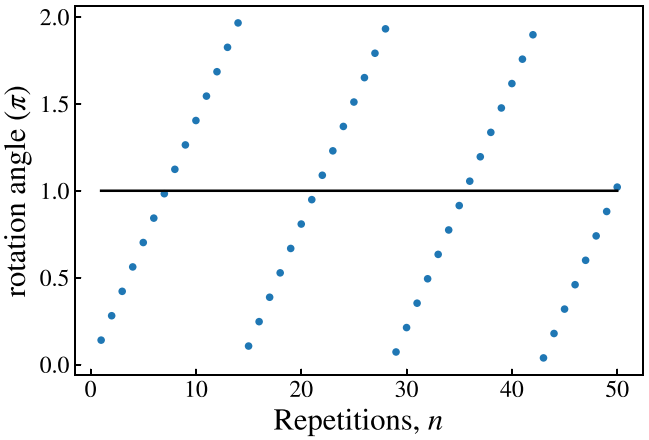

FIG. 4. The rotation angle around the x axis as a function of the repetition n of the adiabatic sequence $W(0, 1; \theta_1^*)$, where θ_1^* is an irrational number approximately equal to 0.17. The irrational rotation angle around the x axis of a single $W(0, 1; \theta_1^*)$ is approximately 0.14π. The black solid line indicates the desired rotation angle π.

desired angle, because the rotation angle of $W(m_a, m_b; \theta_1^*)$ is generally an irrational multiple of 2π; it is approximately 0.14π for $W(0, 1; \theta_1^*)$. Therefore, one can apply repeatedly, say, $W(0, 1; \theta_1^*)$ to achieve the suitable angle π to a desired accuracy. Figure 4 illustrates the procedure by displaying the angle as a function of the repetition n of the sequence $W(0, 1; \theta_1^*)$.

4. Higher-dimensional subspaces

Finally, we show how the holonomic manipulation scheme can be extended to the zero-energy subspaces $\mathcal{D}$ of M ensembles. As discussed at the end of Appendix A, the case of two excitations is particularly attractive, as it yields a series of subspaces $\mathcal{D}$ whose effective dimension is simply equal to the number M of ensembles. This growth of dimension is accompanied by a parallel increase of control parameters, i.e., the amplitudes and phases of the M driving lasers (each one controlling a separate ensemble).

Under this scenario, it is natural to expect that universal manipulation of subspace $\mathcal{D}$ is possible. As a reference, universality for an ensemble of M qubits can be achieved with $O(M)$ gates, which is of the same order of the driving lasers. However, the dimension of the Hilbert space of M qubits quickly becomes much larger than M (the dimension of $\mathcal{D}$). Thus, a zero-energy subspace of M ensembles allows for a very high degree of control.

For a given M, the universality of holonomic operations can be checked by methods analogous to our $M = 2$ discussion, and we have considered explicitly the simplest extension, with $M = 3$ ensembles of two atoms each. First, we determine for any given complex Rabi amplitudes Ω_a, Ω_b, Ω_c three states $|D_j\rangle$ (with $j = 1, 2, 3$) spanning the zero-dimensional subspace. Such states are given by expressions analogous to Eqs. (8) and (9) of the main text. However, the explicit formulas are quite cumbersome and we omit them here.

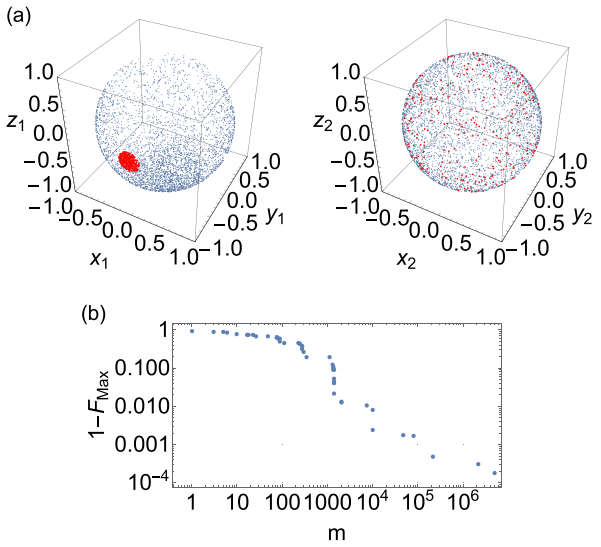

FIG. 5. Application on $|D_1\rangle$ of a random string of holonomies $U_{1,2,3}$, given before Eq. (B13). (a) A visualization of the quantum states produced by the randomly repeated applications of U_i. The points on the right and left spheres are respectively given by (μ_1, ν_1) and (μ_2, ν_2), defined in Eq. (B13). We also highlight in red the states satisfying $|\mu_1 - \pi/2| < 0.05\pi$ and $|\nu_1 - 3\pi/2| < 0.05\pi$. (b) A plot of $F_{\max}(m) = \max\{F(n) : n < m\}$, where $F(n)$ is the fidelity between $|D_3\rangle$ and the state obtained at step n of the random sequence. The value of $F_{\max}(m)$ converges monotonically to 1.

Similar to the case with two ensembles, we can split a path $\mathcal{C}$ into amplitude modulation and phase modulation segments: $\mathcal{C} = \mathcal{C}_\theta + \mathcal{C}_\psi + \mathcal{C}_\phi + \mathcal{C}'_\theta + \mathcal{C}'_\psi + \mathcal{C}'_\phi + \cdots$. These operations are defined according to the parametrization $\Omega_a = \Omega \sin[\theta] e^{i\phi_a}$, $\Omega_b = \Omega \cos[\theta] \sin[\psi] e^{i\phi_b}$, and $\Omega_c = \Omega \cos[\theta] \cos[\psi] e^{i\phi_c}$. In the amplitude modulation segments $\mathcal{C}_\theta(\theta_2, \theta_1; \psi)$, only θ is varied in the range (θ_1, θ_2) keeping ψ unchanged and $\phi_\mu = 0$. The other type of amplitude modulation $\mathcal{C}_\psi(\psi_2, \psi_1; \theta)$ is defined in similar way. In the phase modulation segments $\mathcal{C}(m_a, m_b, m_c; \theta, \psi)$, only the phases ϕ_μ are modulated, from 0 to $2\pi m_\mu$, with θ and ψ held fixed.

To test the universality of holonomic manipulation, we consider the non-Abelian geometric phases $U_1 = U(\mathcal{C}_\phi(1, 0, 0; \pi/6, \pi/6))$, $U_2 = U(\mathcal{C}_\phi(0, 1, 0; \pi/6, \pi/6))$, and $U_3 = U(\mathcal{C}_\phi(0, 0, 1; \pi/6, \pi/6))$. After constructing a long random sequence of these operators, repeatedly applied to $|D_1\rangle$, we represent the resulting family of states in Fig. 5(a). In the plot we rely on the following parametrization:

$$\cos\frac{\mu_1}{2}|D_1\rangle + e^{i\nu_1}\sin\frac{\mu_1}{2}\left(\cos\frac{\mu_2}{2}|D_2\rangle + e^{i\nu_2}\sin\frac{\mu_2}{2}|D_3\rangle\right), \tag{B13}$$

where a general state is specified by azimuthal and polar angles, respectively given by $\mu_{1,2}$ and $\nu_{1,2}$. The representation given in Eq. (B13) is simpler than the Majorana stellar representation [55] and can be extended to general M (when a state is represented by $M - 1$ points on the Bloch sphere). We see in Fig. 5(a) that the random strings of $U_{1,2,3}$ unitaries allow one to fill the (μ_i, ν_i) parameter spaces, which is consistent with universality.

The visual representation in Fig. 5(a) hides any correlation of the points in the two spheres which, in principle, could prevent reaching an arbitrary state. So, we also highlight a subset of points where $(\mu_1, \nu_1) \simeq (\pi/2, 3\pi/2)$. As expected, the corresponding values of (μ_2, ν_2) are still distributed uniformly on the sphere, although with a smaller density. We have tested this property for several other values of (μ_1, ν_1). Finally, panel (b) shows that it is possible to construct a sequence of $U_{1,2,3}$ which transforms an initial state, say, $|D_1\rangle$ to a target state, say, $|D_3\rangle$. ($|D_3\rangle$ is a Dicke state.) The sequence enables one to approximate systematically $|D_3\rangle$. All these properties offer strong evidence of universality for the $U_{1,2,3}$ set of unitary operations.

APPENDIX C: IMPERFECTIONS

1. Decoherence

Quantum states are subject to decoherence, especially when they are manipulated externally such as for quantum information processing. As already mentioned in the main text, however, our scheme is based on the decoherence-free feature of the degenerate zero-energy subspace $\mathcal{D}$ inherited from the quantum Zeno subspace $\mathcal{Z}$, and is fairly insensitive to decoherence effects. To demonstrate it, here we adopt the simplest approach in terms of non-Hermitian Hamiltonian; the detailed mechanism and properties of decoherence are out of the scope of the work. We examine two decoherence effects, the cavity photon decay and the spontaneous emission of atoms, on the fidelity between the symmetric Dicke state and the final state of the adiabatic evolution.

In the ideal case with $g \to \infty$, the dynamics is completely confined within $\mathcal{Z}$, and the photon decay has no effect at all [32,56]. In reality g is finite, and the dynamics is subject to leakage out of $\mathcal{Z}$. It leads to decoherence and results in the reduction of the fidelity. However, this effect is still negligible for reasonably large g as shown by the experimental realizations (see, e.g., [57]) of quantum Zeno dynamics with finite g. In our case, the leakage is mainly through the special zero-energy state in Eq. (18) that persistently exists regardless of the specific values of parameters. Figure 6(a) shows how robust our scheme is against the finite-g effect. The quantum state survives 200 chances ($\kappa T \sim 200$) of photon decay for $g/\Omega = 50$, and more for bigger g. For the plot in Fig. 6(a), we have introduced a non-Hermitian term

$$\hat{H}_\kappa = -i\kappa \hat{c}^\dagger \hat{c} \tag{C1}$$

that is responsible for the cavity photon decay, where the parameter κ denotes the rate. Further, the inset of Fig. 6(a) plots the fidelity between the symmetric Dicke state and the *renormalized* final state. Physically, the renormalized final state describes the component surviving the photon decay and hence the dynamics inside the quantum Zeno subspace $\mathcal{Z}$. The plot in the inset is independent of κ, and the values are the same as the case of $\kappa = 0$ (see Fig. 3 of the main text). This confirms that the photon decay affects our scheme only through the leakage out of $\mathcal{Z}$. In principle, one can analyze the leakage quantitatively by expanding in Ω/g.

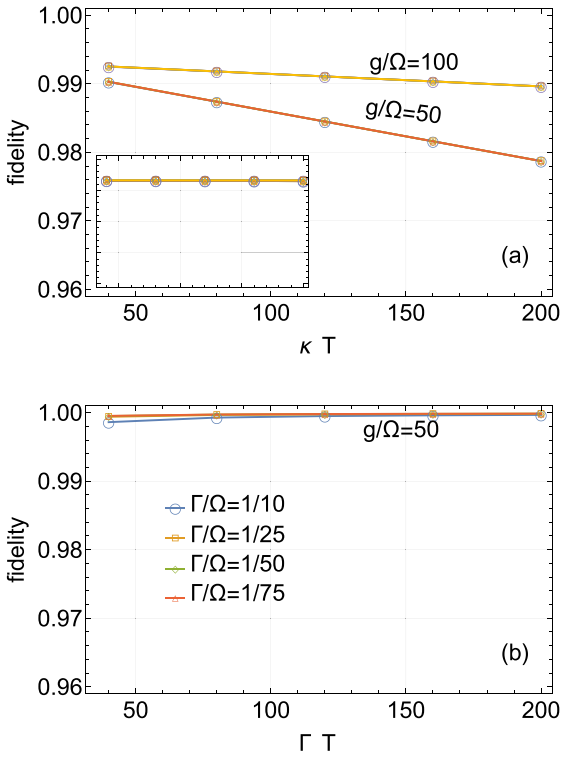

FIG. 6. Fidelity between the final state and the symmetric Dicke state in the presence of decoherence. (a) The fidelity as a function of κT, where κ is the decay rate of the cavity photon and T is the operation time, for two different values (50Ω and 100Ω with $\Omega := \sqrt{\Omega_a^2 + \Omega_b^2}$) of the atom-photon coupling g. Different values of $\kappa/\Omega = 1/10, 1/25, 1/50, 1/75$, corresponding to different symbols (circle, square, diamond, and triangle), result in the same fidelity when plotted as a function of κT. [inset of (a)] Fidelity between the *renormalized* final state and the symmetric Dicke state for both $g/\Omega = 50$ and $g/\Omega = 100$. (b) The fidelity as a function of ΓT, where Γ is the spontaneous decay rate of the atomic level $|2\rangle$, for $g/\Omega = 50$. The fidelity for bigger g (not shown) is even better.

We next turn to the effects of the spontaneous emission of atoms by introducing a non-Hermitian term

$$\hat{H}_\Gamma = -i\Gamma(\hat{a}_2^\dagger \hat{a}_2 + \hat{b}_2^\dagger \hat{b}_2), \tag{C2}$$

where Γ is the spontaneous emission rate. The non-Hermitian term in Eq. (C2) causes irreversible population loss when an atom is in the excited level $|2\rangle$. However, just like a finite detuning of the Rabi amplitudes [37], it also lifts the degeneracy of $\mathcal{D}$ (by an imaginary eigenvalue) since one basis state of $\mathcal{D}$ involves the excited atomic level $|2\rangle$. The other basis state of $\mathcal{D}$ remains at the zero energy. It is clear that if the process in question does not involve the excited atomic level $|2\rangle$, it is resilient to spontaneous decay [54]. The most pronounced example is the generation of the symmetric Dicke state $|\Phi_n^p\rangle$ through adiabatic evolution. Note that the degeneracy lifting is proportional to Γ. It implies that the non-Adiabatic transition to the basis state split by $\hat{H}_\Gamma$ from the zero-energy state is suppressed with increasing Γ. This effect leads to increased fidelity with Γ (to a certain level of Γ) as shown in Fig. 6(b). In general, the overall effects of the spontaneous emission of atoms are less optimistic because the quantum

manipulation in $\mathcal{D}$ involves both basis states. However, the excited atomic level $|2\rangle$ forms only a small portion of the zero-energy subspace $\mathcal{D}$. Therefore, as long as the spontaneous decay rate Γ is sufficiently low (below 10% of the average Rabi amplitude Ω) the scheme maintains the accuracy of manipulations.

2. Inhomogeneity in parameters

So far we have assumed that the parameters within each subensemble are uniform. This allows us to focus on the subspace of totally symmetric wave functions. When parameters deviate for different atoms within an subensemble, the permutation symmetry does not hold any longer. However, as long as the deviations are relatively small, one can still classify the Hilbert space into subspaces corresponding to the irreducible representations of the symmetric group S_m, where m is the number of atoms in a subensemble. The symmetric group S_m consists of permutations, and its irreducible representations are well known and have been widely used since the early days of quantum mechanics [58].

The irreducible representations of the symmetric group are particularly simple when there are two atoms in each subensemble; the relevant symmetric group is thus S_2. Nevertheless, the case is general enough to enable quantum information processing based on the holonomic scheme. In this case, the Hilbert space is composed of two orthogonal subspaces, one $\mathcal{S}$ for totally symmetry wave functions and the other $\mathcal{A}$ for totally antisymmetric wave functions. If the system has two subensembles, the total Hilbert space consists of

$$\mathcal{H} = \mathcal{S}_A \otimes \mathcal{S}_B \oplus \mathcal{S}_A \otimes \mathcal{A}_B \oplus \mathcal{A}_A \otimes \mathcal{S}_B \oplus \mathcal{A}_A \otimes \mathcal{A}_B. \tag{C3}$$

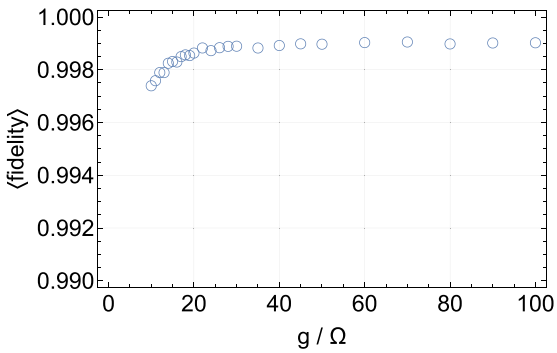

FIG. 7. The average fidelity between the final state and the symmetric Dicke state for inhomogeneous parameters. For the plot, we assumed that the coupling g_j to the cavity photon and the Rabi amplitude Ω_j of the jth atom were uniformly distributed in the relative width of 5%. The fidelity was averaged over 150 realizations of random parameters.

The zero-energy subspace within $\mathcal{S}_A \otimes \mathcal{S}_B$ is three dimensional (including the inert zero-energy state, see Appendix A). The subspaces within $\mathcal{S}_A \otimes \mathcal{A}_B$ and $\mathcal{A}_A \otimes \mathcal{S}_B$ are one dimensional whereas there is no zero-energy state within $\mathcal{A}_A \otimes \mathcal{A}_B$. If the deviations in the parameters are sufficiently small compared with the spectral gap around the zero-energy subspace, the quantum states in the working zero-energy subspace $\mathcal{D}$ are subject to quantum leakage and spread over these five nearly degenerate levels. As shown in Fig. 7, this leakage is typically small if the relative deviations are kept below 5% . Keeping inhomogeneity under a sufficiently low level might be challenging in some systems, especially, in real atomic ensembles where focused laser beams are used to address individual ensembles. In such systems, additional schemes may be required to protect the zero-energy subspace $\mathcal{D}$. We leave it as an open question for future studies.

[1] J. Preskill, Quantum **2**, 79 (2018).
[2] A. Beige, D. Braun, and P. L. Knight, New J. Phys. **2**, 22 (2000).
[3] A. Beige, D. Braun, B. Tregenna, and P. L. Knight, Phys. Rev. Lett. **85**, 1762 (2000).
[4] D. A. Lidar, I. L. Chuang, and K. B. Whaley, Phys. Rev. Lett. **81**, 2594 (1998).
[5] L. Viola and S. Lloyd, Phys. Rev. A **58**, 2733 (1998).
[6] D. Vitali and P. Tombesi, Phys. Rev. A **59**, 4178 (1999).
[7] P. Zanardi, Phys. Lett. A **258**, 77 (1999).
[8] P. W. Shor, Phys. Rev. A **52**, R2493 (1995).
[9] A. M. Steane, Phys. Rev. Lett. **77**, 793 (1996).
[10] M. B. Plenio, V. Vedral, and P. L. Knight, Phys. Rev. A **55**, 67 (1997).
[11] P. Zanardi and M. Rasetti, Phys. Lett. A **264**, 94 (1999).
[12] J. A. Jones, V. Vedral, A. Ekert, and G. Castagnoli, Nature (London) **403**, 869 (2000).
[13] L.-M. Duan, J. I. Cirac, and P. Zoller, Science **292**, 1695 (2001).
[14] E. Sjöqvist, D. M. Tong, L. Mauritz Andersson, B. Hessmo, M. Johansson, and K. Singh, New J. Phys. **14**, 103035 (2012).
[15] K. Toyoda, K. Uchida, A. Noguchi, S. Haze, and S. Urabe, Phys. Rev. A **87**, 052307 (2013).
[16] G. Feng, G. Xu, and G. Long, Phys. Rev. Lett. **110**, 190501 (2013).
[17] A. A. Abdumalikov Jr, J. M. Fink, K. Juliusson, M. Pechal, S. Berger, A. Wallraff, and S. Filipp, Nature (London) **496**, 482 (2013).
[18] C. Zu, W.-B. Wang, L. He, W.-G. Zhang, C.-Y. Dai, F. Wang, and L.-M. Duan, Nature (London) **514**, 72 (2014).
[19] Y. Xu, W. Cai, Y. Ma, X. Mu, L. Hu, T. Chen, H. Wang, Y. P. Song, Z.-Y. Xue, Z.-q. Yin, and L. Sun, Phys. Rev. Lett. **121**, 110501 (2018).
[20] Y.-Y. Huang, Y.-K. Wu, F. Wang, P.-Y. Hou, W.-B. Wang, W.-G. Zhang, W.-Q. Lian, Y.-Q. Liu, H.-Y. Wang, H.-Y. Zhang, L. He, X.-Y. Chang, Y. Xu, and L.-M. Duan, Phys. Rev. Lett. **122**, 010503 (2019).
[21] Y. Li, P. Zhang, P. Zanardi, and C. P. Sun, Phys. Rev. A **70**, 032330 (2004).
[22] M. H. Freedman, Proc. Natl. Acad. Sci. U.S.A. **95**, 98 (1998).
[23] A. Kitaev, Ann. Phys. (NY) **303**, 2 (2003).

[24] C. Nayak, S. H. Simon, A. Stern, M. Freedman, and S. Das Sarma, Rev. Mod. Phys. **80**, 1083 (2008).

[25] V. Mourik, K. Zuo, S. M. Frolov, S. R. Plissard, E. P. A. M. Bakkers, and L. P. Kouwenhoven, Science **336**, 1003 (2012).

[26] M. T. Deng, C. L. Yu, G. Y. Huang, M. Larsson, P. Caroff, and H. Q. Xu, Nano Lett. **12**, 6414 (2012).

[27] A. Das, Y. Ronen, Y. Most, Y. Oreg, M. Heiblum, and H. Shtrikman, Nat. Phys. **8**, 887 (2012).

[28] S. Nadj-Perge, I. K. Drozdov, J. Li, H. Chen, S. Jeon, J. Seo, A. H. MacDonald, B. A. Bernevig, and A. Yazdani, Science **346**, 602 (2014).

[29] H. Bartolomei, M. Kumar, R. Bisognin, A. Marguerite, J.-M. Berroir, E. Bocquillon, B. Plaçais, A. Cavanna, Q. Dong, U. Gennser, Y. Jin, and G. Fève, Science **368**, 173 (2020).

[30] Our scheme is not limited to real atoms but also applies to other systems as long as the constituent elements have the Λ-type level structure. Common examples include the nitrogen-vacancy center in diamonds [18,37], quantum dots in microcavities [35], superconducting circuit quantum electrodynamics systems [59–62], and trapped ions [43,44].

[31] Y. Aharonov and J. Anandan, Phys. Rev. Lett. **58**, 1593 (1987).

[32] P. Facchi and S. Pascazio, Phys. Rev. Lett. **89**, 080401 (2002).

[33] J. L. Wu and S. L. Su, J. Phys. A: Math. Theor. **52**, 335301 (2019).

[34] X.-K. Song, H. Zhang, Q. Ai, J. Qiu, and F.-G. Deng, New J. Phys. **18**, 023001 (2016).

[35] A. Imamoğlu, D. D. Awschalom, G. Burkard, D. P. DiVincenzo, D. Loss, M. Sherwin, and A. Small, Phys. Rev. Lett. **83**, 4204 (1999).

[36] V. A. Mousolou and E. Sjöqvist, J. Phys. A: Math. Theor. **51**, 475303 (2018).

[37] W. Yang, Z. Xu, M. Feng, and J. Du, New J. Phys. **12**, 113039 (2010).

[38] X.-Q. Shao, L. Chen, S. Zhang, Y.-F. Zhao, and K.-H. Yeon, Europhys. Lett. **90**, 50003 (2010).

[39] Y.-H. Chen, Y. Xia, and J. Song, Quantum Info. Process. **13**, 1857 (2014).

[40] J.-L. Wu, X. Ji, and S. Zhang, Sci. Rep. **7**, 46255 (2017).

[41] J. Simon, H. Tanji, S. Ghosh, and V. Vuletić, Nat. Phys. **3**, 765 (2007).

[42] J. M. Weiner, K. C. Cox, J. G. Bohnet, and J. K. Thompson, Phys. Rev. A **95**, 033808 (2017).

[43] D. B. Hume, C. W. Chou, T. Rosenband, and D. J. Wineland, Phys. Rev. A **80**, 052302 (2009).

[44] Y. Lin, J. P. Gaebler, F. Reiter, T. R. Tan, R. Bowler, Y. Wan, A. Keith, E. Knill, S. Glancy, K. Coakley, A. S. Sørensen, D. Leibfried, and D. J. Wineland, Phys. Rev. Lett. **117**, 140502 (2016).

[45] Commonly called the chiral symmetry in condensed matter physics and high energy physics, the anti-symmetry is not a "symmetry" in the usual sense because the Hamiltonian does not commute with the symmetry operator.

[46] E. M. Purcell, Phys. Rev. **69**, 674 (1946), special issue, Proceedings of the American Physical Society.

[47] M. V. Berry, Proc. R. Soc. London A **392**, 45 (1984).

[48] F. Wilczek and A. Zee, Phys. Rev. Lett. **52**, 2111 (1984).

[49] G. Tóth, J. Opt. Soc. Am. B **24**, 275 (2007).

[50] G. Tóth, W. Wieczorek, R. Krischek, N. Kiesel, P. Michelberger, and H. Weinfurter, New J. Phys. **11**, 083002 (2009).

[51] I. Apellaniz, B. Lücke, J. Peise, C. Klempt, and G. Tóth, New J. Phys. **17**, 083027 (2015).

[52] L. Pezze, A. Smerzi, M. K. Oberthaler, R. Schmied, and P. Treutlein, Rev. Mod. Phys. **90**, 035005 (2018).

[53] M. J. Holland and K. Burnett, Phys. Rev. Lett. **71**, 1355 (1993).

[54] N. V. Vitanov, A. A. Rangelov, B. W. Shore, and K. Bergmann, Rev. Mod. Phys. **89**, 015006 (2017).

[55] E. Majorana, Nuovo Cimento **9**, 43 (1932).

[56] P. Facchi, G. Marmo, and S. Pascazio, J. Phys.: Conf. Ser. **196**, 012017 (2009).

[57] F. Schäfer, I. Herrera, S. Cherukattil, C. Lovecchio, F. Cataliotti, F. Caruso, and A. Smerzi, Nat. Commun. **5**, 3194 (2014).

[58] E. P. Wigner, *Group Theory and its Application to the Quantum Mechanics of Atomic Spectra* (Academic Press, New York, 1959).

[59] A. Wallraff, D. I. Schuster, A. Blais, L. Frunzio, R.-S. Huang, J. Majer, S. Kumar, S. M. Girvin, and R. J. Schoelkopf, Nature (London) **431**, 162 (2004).

[60] A. A. Houck, D. I. Schuster, J. M. Gambetta, J. A. Schreier, B. R. Johnson, J. M. Chow, L. Frunzio, J. Majer, M. H. Devoret, S. M. Girvin *et al.*, Nature (London) **449**, 328 (2007).

[61] Z.-L. Xiang, S. Ashhab, J. Q. You, and F. Nori, Rev. Mod. Phys. **85**, 623 (2013).

[62] P. Forn-Díaz, L. Lamata, E. Rico, J. Kono, and E. Solano, Rev. Mod. Phys. **91**, 025005 (2019).